

Elastic fingering in rotating Hele-Shaw flowsGabriel D. Carvalho,¹ Hermes Gadêlha,² and José A. Miranda^{1,*}¹*Departamento de Física, Universidade Federal de Pernambuco, Recife, Pernambuco 50670-901, Brazil*²*Wolfson Centre for Mathematical Biology, Mathematical Institute, University of Oxford, Oxford OX2 6GG, United Kingdom*

(Received 6 March 2014; published 21 May 2014)

The centrifugally driven viscous fingering problem arises when two immiscible fluids of different densities flow in a rotating Hele-Shaw cell. In this conventional setting an interplay between capillary and centrifugal forces makes the fluid-fluid interface unstable, leading to the formation of fingered structures that compete dynamically and reach different lengths. In this context, it is known that finger competition is very sensitive to changes in the viscosity contrast between the fluids. We study a variant of such a rotating flow problem where the fluids react and produce a gellike phase at their separating boundary. This interface is assumed to be elastic, presenting a curvature-dependent bending rigidity. A perturbative weakly nonlinear approach is used to investigate how the elastic nature of the interface affects finger competition events. Our results unveil a very different dynamic scenario, in which finger length variability is not regulated by the viscosity contrast, but rather determined by two controlling quantities: a characteristic radius and a rigidity fraction parameter. By properly tuning these quantities one can describe a whole range of finger competition behaviors even if the viscosity contrast is kept unchanged.

DOI: [10.1103/PhysRevE.89.053019](https://doi.org/10.1103/PhysRevE.89.053019)

PACS number(s): 47.15.gp, 47.70.Fw, 47.54.-r, 47.20.Ma

I. INTRODUCTION

The traditional viscous fingering instability [1,2] is driven by the viscosity difference between fluids. More precisely, it manifests itself when a less viscous fluid pushes a more viscous one in the narrow gap separating parallel plates of a motionless Hele-Shaw cell. Under radial flow circumstances [3–9] an initially circular fluid-fluid interface deforms, and patterned structures presenting multiple fingertip splitting emerge.

An alternative form of fingering instability in Hele-Shaw geometry arises when there exists a difference in density between the fluids, and the cell is put in motion. This occurs when a fluid, surrounded by another of lower density, is located in a Hele-Shaw cell that rotates about an axis perpendicular to the cell plates. Centrifugal forces act upon the density difference between the fluids, and a morphological instability results. A great variety of patterned shapes is obtained in this rotating Hele-Shaw setup [10–18], leading to fingering structures that are very distinct from the ones detected in viscosity-driven Hele-Shaw flows.

In contrast to the viscosity-driven problem the most prominent pattern-forming mechanism in the density-driven, rotating Hele-Shaw case is not finger tip splitting, but the competition (or the finger length variability) among the interfacial fingers. Weakly nonlinear analysis [19] and fully nonlinear numerical simulations [13,20] have verified that the viscosity contrast A [dimensionless viscosity difference between the fluids, where $-1 \leq A \leq 1$ as defined in Eq. (2)] plays a crucial role in determining the resulting fingered structures, in the sense that finger competition dynamics changes significantly when the magnitude and sign of A are varied. It has been found that increasingly larger values of $A > 0$ ($A < 0$) lead to enhanced competition among outward- (inward-) pointing fingers. In addition, finger competition is significantly suppressed when $A \rightarrow 0$.

In this work we revisit the rotating Hele-Shaw cell problem in a different scenario: inspired by recent studies in viscosity-driven radial Hele-Shaw flows [21–24], we consider that the interface separating the fluids acts like an elastic membrane which has a curvature-dependent bending rigidity. The formation of a flexible gellike layer between the fluids is induced by a chemical reaction that occurs at the interface. In this framework, interfacial instabilities can be triggered by the own elastic nature of the fluid-fluid boundary. In Refs. [21–24] it has been shown that the existence of an elastic interface has a strong impact on the dynamics and morphology of the emerging interfacial patterns. In fact, the conventional branched, tip-splitting patterns observed in Refs. [3–9] are replaced by a variety of other interfacial forms, exhibiting mushroom-shaped structures and tentacle-like fingers. It is worth noting that a similar type of investigation focusing on the influence of the interface elasticity on pattern-forming phenomena under the centrifugally driven flow in rotating Hele-Shaw cells still needs to be performed. This is in fact the main purpose of our present work.

Here we are interested in examining the influence of the elastic interface on the most relevant dynamic features of the centrifugally driven fingering patterns. We focus our attention on investigating how elasticity effects interfere in the finger competition events that usually arise in rotating Hele-Shaw flows. The role of the viscosity contrast in determining finger competition behavior in the presence of an elastic interface is also discussed. To address these important issues we study both linear and weakly nonlinear stages of the dynamics. This is done by employing a second-order mode-coupling perturbative scheme [8,24] which offers useful analytical insights into the onset of pattern formation and fingering in this complex elastic interface system.

II. WEAKLY NONLINEAR EQUATIONS

Consider a Hele-Shaw cell of gap spacing b containing two immiscible, incompressible, viscous fluids (see Fig. 1).

*jme@df.ufpe.br

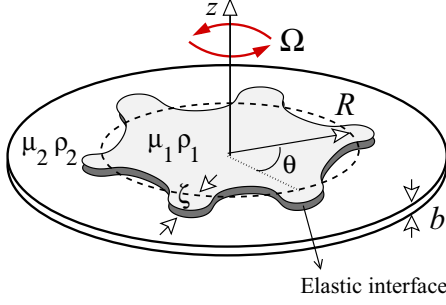


FIG. 1. (Color online) Perspective view of a rotating Hele-Shaw cell with an elastic interface separating fluids 1 and 2.

Denote the densities and viscosities of the inner and outer fluids, respectively as ρ_1, μ_1 and ρ_2, μ_2 . We focus on the centrifugally induced motion where $\rho_1 > \rho_2$ but allow the inner fluid to be either more or less viscous than the outer fluid. The cell rotates with constant angular velocity Ω about an axis perpendicular to the plates (z axis) and passing through the center of the cell. Due to a chemical reaction there exists a gellike interface separating the two fluids. As in Refs. [22–24] we treat the interface as an elastic membrane, presenting a curvature-dependent bending rigidity.

The perturbed fluid-fluid interface is described as $\mathcal{R}(\theta, t) = R + \zeta(\theta, t)$, where θ represents the azimuthal angle, and R is the radius of the initially circular fluid-fluid interface at $t = 0$. Here $\zeta(\theta, t) = \sum_{n=-\infty}^{+\infty} \zeta_n(t) \exp(in\theta)$ denotes the net interface perturbation with Fourier amplitudes $\zeta_n(t)$ and discrete wave numbers n . Our perturbative approach keeps terms up to the second order in ζ . In the Fourier expansion of ζ we include the $n = 0$ mode to maintain the area of the perturbed shape independent of the perturbation ζ . Mass conservation imposes that the zeroth mode is written in terms of the other modes as $\zeta_0 = -(1/2R) \sum_{n \neq 0} |\zeta_n(t)|^2$.

For the effectively two-dimensional geometry of the Hele-Shaw cell, the flow velocity $\mathbf{v}_j = -\nabla\phi_j$, where ϕ_j represents the velocity potential in fluids $j = 1, 2$. The equation of motion of the interface is given by Darcy's law [1, 2], properly augmented by a centrifugally driven term [10, 11]

$$A \left(\frac{\phi_2 + \phi_1}{2} \right) + \left(\frac{\phi_2 - \phi_1}{2} \right) = \frac{b^2}{12(\mu_1 + \mu_2)} \left[\frac{1}{2}(\rho_1 - \rho_2)\Omega^2 r^2 - \Delta p \right], \quad (1)$$

where the dimensionless parameter

$$A = \frac{\mu_2 - \mu_1}{\mu_2 + \mu_1} \quad (2)$$

is the viscosity contrast, p_j represents the pressure, and r denotes the radial distance from the axis of rotation. Additionally, we have that

$$\Delta p = (p_1 - p_2)|_{r=\mathcal{R}} - (p_1 - p_2)|_{r=R}, \quad (3)$$

where $(p_1 - p_2)|_{r=\mathcal{R}}$ denotes the pressure jump on the perturbed interface, while $(p_1 - p_2)|_{r=R}$ represents the pressure jump on the unperturbed interface.

To include the contributions coming from the elastic nature of the fluid-fluid interface, similarly to what was done in

Refs. [22–24], we consider a generalized Young-Laplace pressure boundary condition, which expresses the pressure jump across the perturbed fluid-fluid interface as

$$(p_1 - p_2)|_{r=\mathcal{R}} = -\frac{1}{2}v''' \kappa^2 \kappa_s^2 - v''(3\kappa \kappa_s^2 + \frac{1}{2}\kappa^2 \kappa_{ss}) - v'(\frac{1}{2}\kappa^4 + 3\kappa_s^2 + 2\kappa \kappa_{ss}) - v(\frac{1}{2}\kappa^3 + \kappa_{ss}), \quad (4)$$

where

$$v = v(\kappa) = v_0 [C e^{-\lambda^2 \kappa^2} + 1 - C] \quad (5)$$

is the bending rigidity function, v_0 is the maximum rigidity that expresses the largest resistance to disturbances, and $0 \leq C < 1$ is the rigidity fraction, which measures the fraction of intramolecular bonds broken through surface deformation. Note that the constant rigidity limit is reached in Eq. (5) by setting $C = 0$. In Eq. (5) κ denotes the interface curvature in the plane of the cell, which in polar coordinates is given by [8]

$$\kappa = \frac{[r^2 + 2(\frac{\partial r}{\partial \theta})^2 - r \frac{\partial^2 r}{\partial \theta^2}]}{[r^2 + (\frac{\partial r}{\partial \theta})^2]^{3/2}}, \quad (6)$$

and $\lambda > 0$ is a characteristic radius [22]. We can think of the quantity $1/\lambda$ as being a characteristic curvature beyond which $v(\kappa)$ has a substantial decrease. In Eq. (4) the primes indicate derivatives with respect to the curvature κ , while the subscripts of κ indicate derivatives with respect to the arc length s .

To obtain a mode-coupling differential equation for the evolution of the perturbation amplitudes, we adapt a weakly nonlinear approach originally developed to study the dynamics in motionless Hele-Shaw flows induced by injection [8] to the current rotating cell problem presenting an elastic fluid-fluid interface. First, we define Fourier expansions for the velocity potentials, which obey Laplace's equation $\nabla^2 \phi_j = 0$. Then we express ϕ_j in terms of the perturbation amplitudes ζ_n by considering the kinematic boundary condition $\mathbf{n} \cdot \nabla \phi_1 = \mathbf{n} \cdot \nabla \phi_2$, which refers to the continuity of the normal velocity across the interface. Substituting these relations, and the modified pressure jump condition Eq. (4) into Eq. (1), always keeping terms up to second order in ζ , and Fourier transforming, yields the *dimensionless* mode-coupling equation (for $n \neq 0$)

$$\dot{\zeta}_n = \Lambda(n)\zeta_n + \sum_{m \neq 0} [F(n, m)\zeta_m \zeta_{n-m} + G(n, m)\dot{\zeta}_m \zeta_{n-m}], \quad (7)$$

where the overdot denotes total time derivative,

$$\Lambda(n) = |n| \left\{ 1 + \frac{B}{2}(n^2 - 1)[A_1(C, \lambda)(n^2 + 1) + A_2(C, \lambda)] \right\} \quad (8)$$

is the linear growth rate, and

$$B = \frac{v_0}{(\rho_1 - \rho_2)\Omega^2 R^5} \quad (9)$$

measures the ratio of elastic to centrifugal forces,

$$A_1(C, \lambda) = C e^{-\lambda^2} (-4\lambda^4 + 10\lambda^2 - 2) - 2(1 - C) \quad (10)$$

and

$$A_2(C, \lambda) = Ce^{-\lambda^2}(8\lambda^4 - 22\lambda^2 + 5) + 5(1 - C). \quad (11)$$

The second-order mode-coupling terms are given by

$$F(n, m) = |n| \left\{ \frac{1}{2} - B [Ce^{-\lambda^2}(B_1(n, m) + \lambda^2 B_2(n, m) + \lambda^4 B_3(n, m) + 2\lambda^6 B_4(n, m)) + (1 - C)B_1(n, m)] \right\} \quad (12)$$

and

$$G(n, m) = A|n|[1 - \text{sgn}(nm)] - 1, \quad (13)$$

where the sgn function equals ± 1 according to the sign of its argument. The expressions for the functions $B_1(n, m)$, $B_2(n, m)$, $B_3(n, m)$, and $B_4(n, m)$ are given in the Appendix. Note that in Eqs. (7)–(13) lengths are rescaled by R and time by R/U , where $U = [b^2 R(\rho_1 - \rho_2)\Omega^2]/[12(\mu_1 + \mu_2)]$ is a characteristic velocity. From this point on we use the dimensionless version of all the equations.

Equations (7)–(13) represent the mode-coupling equations of the elastic fingering instability problem in a rotating Hele-Shaw cell, considering that the interface has a curvature-dependent bending rigidity. This set of nonlinear equations allows one to investigate analytically how the important mechanism of finger competition respond to the interplay between centrifugal and elastic forces at the fluid-fluid boundary.

III. ELASTIC INTERFACE EFFECTS: LINEAR AND NONLINEAR REGIMES

A. Linear stage

For the sake of completeness, before discussing the inherently nonlinear effects related to the finger competition dynamics, we briefly discuss the linear part of Eq. (7), more specifically the linear growth rate $\Lambda(n)$. The first term in Eq. (8) is connected to the destabilizing centrifugal force, while the second term expresses the bending rigidity contribution. For a given n , in the limit of constant rigidity ($C = 0$) the quantity $[A_1(C, \lambda)(n^2 + 1) + A_2(C, \lambda)]$ is negative, and the bending forces tend to stabilize the interface. In this case, the parameter ν_0 acts like an effective surface tension, similarly to what one has in the usual rotating Hele-Shaw problem [10–18]. However, if $0 < C < 1$ the quantity $[A_1(C, \lambda)(n^2 + 1) + A_2(C, \lambda)]$ can become positive, and the effect of the curvature-dependent bending rigidity may lead to interface destabilization. In this work we focus on situations in which $-1 \leq A \leq 1$ and $0 < C \leq 0.5$ [we point out that $\Lambda(n)$ can be unbound if $C > 0.5$], so that bending forces are destabilizing.

We stress that the values we take for our parameters throughout this work are consistent with typical physical quantities used in real experiments in rotating Hele-Shaw cells [11,12,14,16] and with related experimental and theoretical studies involving the development of the elastic fingering instability in injection-driven radial flow geometry [21–23].

The typical destabilizing nature of the bending forces is expressed by Fig. 2, which plots the linear growth rate $\Lambda(n)$ as a function of the Fourier mode n , for $C = 0.1, 0.3$, and 0.5 , and $\lambda = 1$ (dotted curves) and 0.7 (dashed curves). We take

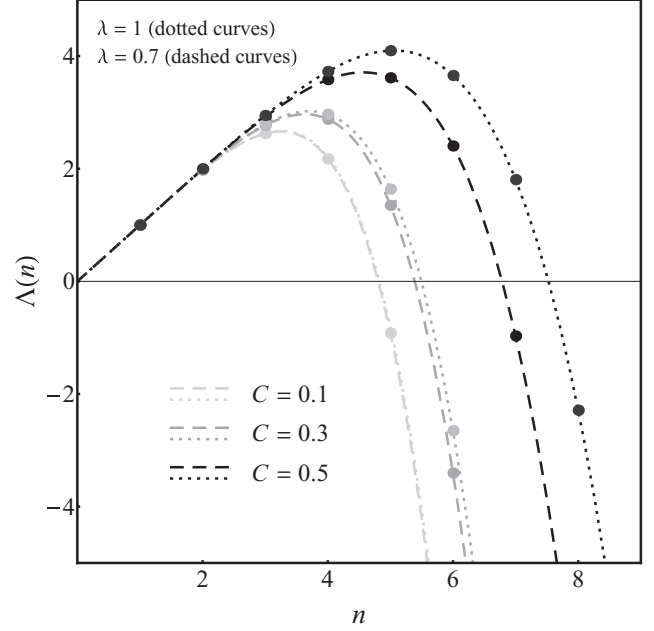


FIG. 2. Linear growth rate $\Lambda(n)$ as a function of mode n , for three values of C and two values of λ . Here $B = 2.5 \times 10^{-3}$.

$B = 2.5 \times 10^{-3}$. By inspecting Fig. 2 it is clear that, for a fixed value of λ , both the band of unstable modes and the mode of largest growth rate increase as C is increased. This is due to the fact that the bending rigidity function $\nu(\kappa)$ varies linearly with C . For a fixed C and variable λ we have regions in which the band of unstable modes and the mode of largest growth rate increase (see Fig. 2), or in which both decrease. This occurs because $\nu(\kappa)$ depends on λ as a Gaussian [Eq. (5)]. Finally, it is also evident that when $C \rightarrow 0$ the dotted and dashed curves tend to overlap, so that the width of the band of unstable modes tends to a minimal value.

B. Weakly nonlinear stage

In this section we use our mode-coupling approach to investigate the interface evolution at second order. We demonstrate the usefulness of our weakly nonlinear analysis in elucidating key aspects related to the finger competition behavior under the action of interfacial elastic effects. To simplify our discussion we rewrite the net perturbation in terms of cosine and sine modes

$$\zeta(\theta, t) = \zeta_0 + \sum_{n=1}^{\infty} [a_n(t) \cos(n\theta) + b_n(t) \sin(n\theta)], \quad (14)$$

where $a_n = \zeta_n + \zeta_{-n}$ and $b_n = i(\zeta_n - \zeta_{-n})$ are real-valued. Without loss of generality we may choose the phase of the fundamental mode so that $a_n > 0$ and $b_n = 0$.

We focus on the effects of the interface elasticity on finger competition events. We follow Ref. [8] and consider finger length variability as a measure of the competition among fingers. Within our approach the finger competition mechanism can be described by the influence of a fundamental mode n , assuming n is even, on the growth of its subharmonic mode $n/2$. By using Eqs. (7)–(13) the equations of motion for

the subharmonic mode can be written as

$$\dot{a}_{n/2} = \{\lambda(n/2) + \mathcal{C}(n)a_n\}a_{n/2}, \quad (15)$$

$$\dot{b}_{n/2} = \{\lambda(n/2) - \mathcal{C}(n)a_n\}b_{n/2}, \quad (16)$$

where

$$\mathcal{C}(n) = \frac{1}{2} \left\{ \left[F\left(-\frac{n}{2}, \frac{n}{2}\right) + \lambda(n/2)G\left(\frac{n}{2}, -\frac{n}{2}\right) \right] + \left[F\left(\frac{n}{2}, n\right) + \lambda(n)G\left(\frac{n}{2}, n\right) \right] \right\} \quad (17)$$

is the finger competition function. Observing Eqs. (15) and (16), and recalling that $a_n > 0$, we verify that $\mathcal{C}(n) > 0$ increases the growth of the cosine subharmonic $a_{n/2}$, while inhibiting growth of its sine subharmonic $b_{n/2}$. The result is an increased variability among the lengths of fingers of fluid 1 pushing the less dense fluid 2. This effect describes enhanced competition of the outward-pointing fingers of fluid 1. Sine modes $b_{n/2}$ would vary the lengths of fingers of fluid 2 penetrating into fluid 1, but it is clear from Eq. (16) that their growth is suppressed if $\mathcal{C}(n) > 0$.

Reversing the sign of $\mathcal{C}(n)$ would exactly reverse these conclusions, such that modes $b_{n/2}$ would be favored over modes $a_{n/2}$. Therefore, $\mathcal{C}(n) < 0$ would indicate increased competition among the inward moving fingers of fluid 2. Regardless of its sign, the magnitude of the function $\mathcal{C}(n)$ as given by Eq. (17) measures the strength of the competition: increasingly larger values of $\mathcal{C}(n)$ lead to enhanced finger competition.

To examine the influence of the elastic interface effects on finger competition at second order, in Fig. 3 we plot the finger competition function $\mathcal{C}(n)$ [as given by Eq. (17)] in terms of λ , for three characteristic values of the viscosity contrast A , $B = 2.5 \times 10^{-3}$, and $C = 0.5$. As in Ref. [19], to observe growth of the fundamental mode and also to allow growth of its

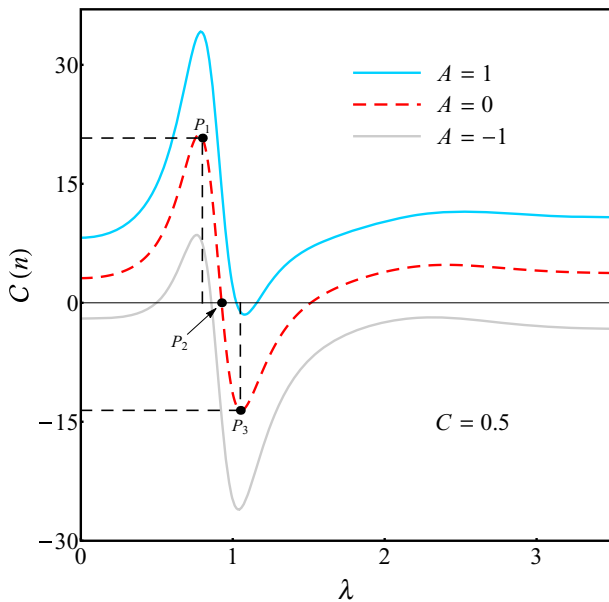


FIG. 3. (Color online) Finger competition function $\mathcal{C}(n)$ plotted in terms of λ , for $B = 2.5 \times 10^{-3}$, $C = 0.5$, and three values of $A = 1, 0$, and -1 .

subharmonic, we carry out our analysis considering that mode n obeys the condition $\Lambda(n) = 0$. The most interesting feature revealed by Fig. 3 is the fact that, no matter what value of A one considers, for a given fixed value of the viscosity contrast the function $\mathcal{C}(n)$ can be positive, negative, or zero as one varies the magnitude of λ . This is in striking contrast to what is observed in the conventional rotating Hele-Shaw problem (for which the interface is not elastic) [10–18], where the finger competition function can change only if the viscosity contrast is varied. This means that under the consideration of an elastic interface the parameters λ and C , and *not* the viscosity contrast A , determine the finger competition behavior. For instance, in Fig. 3 when $A = 0$ one can see situations in which we have (1) enhanced competition among outward-pointing fingers [see point P_1 where $\mathcal{C}(n)$ is large and positive]; (2) restrained competition of both outward- and inward-pointing fingers [see point P_2 where $\mathcal{C}(n)$ is zero]; and (3) enhanced competition among inward-pointing fingers [see point P_3 where $\mathcal{C}(n)$ is large and negative]. In fact, this is true for all values of the viscosity contrast A . Notice that the behaviors for $A = 1$ and $A = -1$ are also illustrated in Fig. 3. It is worth pointing out that for a given value of A in Fig. 3, the finger competition function $\mathcal{C}(n)$ does not change sign if larger values of λ are considered.

In order to verify the predictions indicated in the discussion of Fig. 3, in Fig. 4 we plot the weakly nonlinear evolution of the interfaces for $A = 0$ that correspond to the points P_1 where $\lambda = 0.8$ [Fig. 4(a)], P_2 where $\lambda = 0.926$ [Fig. 4(b)], and P_3 where $\lambda = 1.05$ [Fig. 4(c)]. In Fig. 4 we take the initial perturbation amplitudes as $a_n(0) = 1/400$ and $a_{n/2}(0) = b_{n/2}(0) = 1/800$. In addition, as in Fig. 3 $B = 2.5 \times 10^{-3}$, and $C = 0.5$. All patterns shown in Fig. 4 are plotted for $0 \leq t \leq 1.25$, in equal time intervals $\Delta t = 0.125$.

By inspecting Figs. 4(a)–(c) we observe the evolution of initially nearly circular shapes that deform and develop fingers as time progresses. It is evident that in Fig. 4(a) one notices the enhanced competition among outward-pointing fingers. On the other hand, in Fig. 4(b) one clearly observes that the lengths of the outward-moving fingers are not that different. This is also true for the inward-moving fingers, which have similar sizes. Finally, by examining Fig. 4(c) one sees that there is greater finger length variability among the inward-pointing fingers. All these observations are in line with the predictions extracted from Fig. 3. We stress that we have verified similar kind of behaviors for any other values of the viscosity contrast A .

To illustrate these finger competition features in a more quantitative fashion, in Fig. 5 we take the same physical parameters used in Fig. 4 and plot the dimensionless radial coordinate \mathcal{R} of the finger tips for each inward- and outward-pointing fingers, in terms of the polar angle θ at time $t = t_f$. The finger competition features we have discussed above, by visually inspecting the patterns shown in Fig. 4, are fully confirmed by Fig. 5: even though the viscosity contrast is constant ($A = 0$), by changing the value of λ we do recover the cases in which one obtains enhanced competition among outward fingers [Fig. 5(a)], suppressed competition of both inward and outward fingers [Fig. 5(b)], and favored competition among inward fingers [Fig. 5(c)]. This indicates that, in the presence of an elastic interface, the competition among the emerging fingering structures is primarily determined by the parameters λ and C , and not by the viscosity contrast.

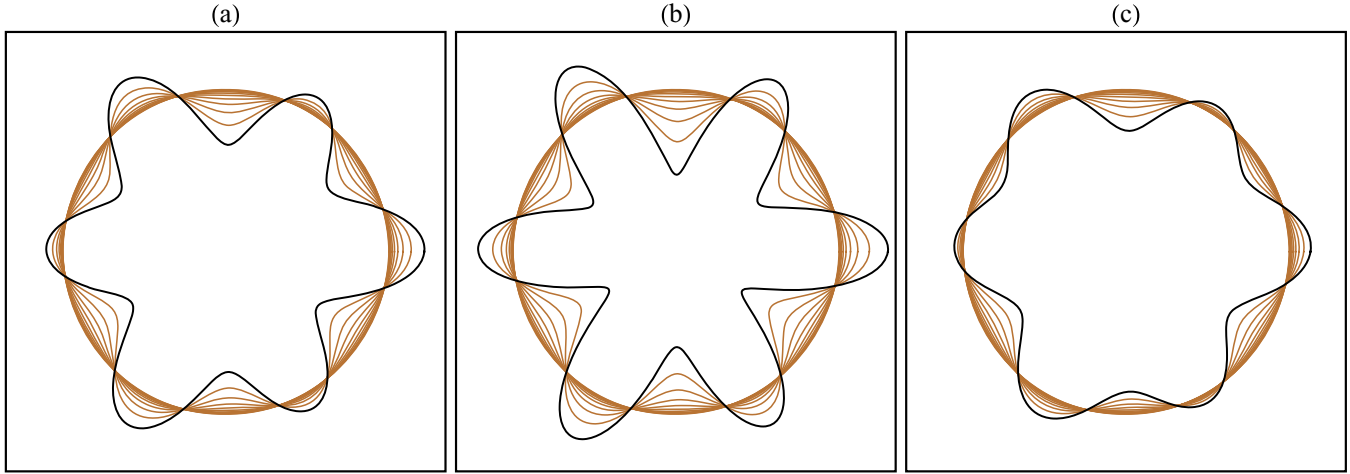


FIG. 4. (Color online) Snapshots of the evolving interface for the interaction of the fundamental mode $n = 6$ and its subharmonic mode $n = 3$ for the situations corresponding to points P_1 (a) $\lambda = 0.8$, P_2 (b) $\lambda = 0.926$, and P_3 (c) $\lambda = 1.05$ that have been indicated in Fig. 3 for $A = 0$. The interfaces are plotted in intervals of $t_f/10$, where $t_f = 1.25$ is the final time. The darker interfaces correspond to $t = t_f$.

We proceed by investigating the behavior of the finger competition function $\mathcal{C}(n)$ when we consider a fixed value of A and vary the magnitude of the rigidity fraction C . Without loss of generality in Fig. 6 we take $A = 0$ and depict how $\mathcal{C}(n)$ responds to variations in λ , when C decreases from 0.5 to 0.1. As in Fig. 3, we consider that $B = 2.5 \times 10^{-3}$. From Fig. 6 we see that when $C = 0.5$, one reproduces the $\mathcal{C}(n)$ curve already shown in Fig. 3 for $A = 0$: initially the competition function is positive, reaches a maximum value, and then starts to decrease. Eventually, $\mathcal{C}(n)$ crosses zero, begins to assume negative values, and reaches a minimum. After that, it crosses zero again and becomes positive for larger values of λ . When $C = 0.4$ a similar type of general behavior is detected, with $\mathcal{C}(n)$ assuming positive, zero, and negative values. However, if C keeps decreasing, for instance, when $C = 0.3$ or $C = 0.2$, the function $\mathcal{C}(n)$ varies in such a way that it still oscillates but assumes just positive values as λ is changed. Finally, for smaller values of C , say, for $C = 0.1$ (dashed horizontal line), the competition function is basically insensitive to variations

in λ . In the limit $C \rightarrow 0$ we have verified that $\mathcal{C}(n)$ also does not depend on λ , and we recover something similar to the conventional rotating Hele-Shaw case [10–18] in which the constant bending rigidity works like an effective surface tension, and where $\mathcal{C}(n)$ varies only if A is changed. We emphasize that all the findings of Fig. 6 (obtained for $A = 0$) are quite general and can be reproduced for any allowed value of the viscosity contrast A .

Other useful information can be extracted from Fig. 7 that shows the variation of the finger competition function $\mathcal{C}(n)$ as the viscosity contrast is varied ($-1 \leq A \leq 1$), for $C = 0.5$ and the three values of λ that have been used to plot Figs. 4 and 5: 0.8, 0.926, and 1.05. As before we take $B = 2.5 \times 10^{-3}$. Despite the dominant, nonmonotonic response of λ while determining the finger competition, as clearly shown in Fig. 3, the monotonicity and linearity of $\mathcal{C}(n)$ with the viscosity contrast A are still preserved. This linearity of the finger competition with the viscosity contrast is reminiscent from the classical rotating Hele-Shaw system for a nonelastic in-

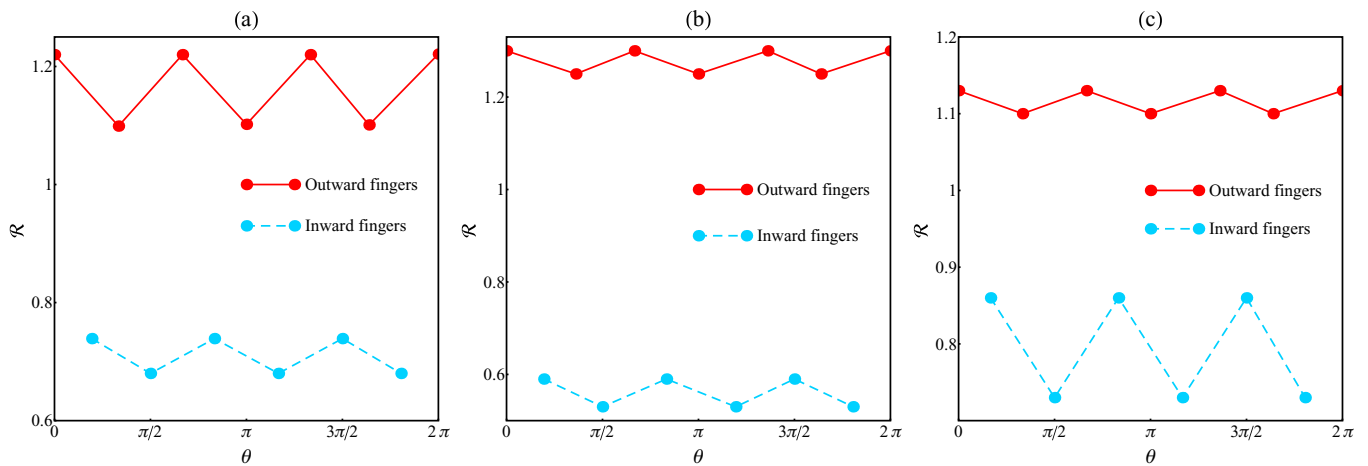


FIG. 5. (Color online) Dimensionless radial coordinate \mathcal{R} of the finger tips for each inward- and outward-pointing fingers, as a function of the polar angle θ , when (a) $\lambda = 0.8$, (b) $\lambda = 0.9286$, and (c) $\lambda = 1.05$. These data are taken from the corresponding patterns plotted in Figs. 4(a)–(c) at $t = t_f$, and $A = 0$.

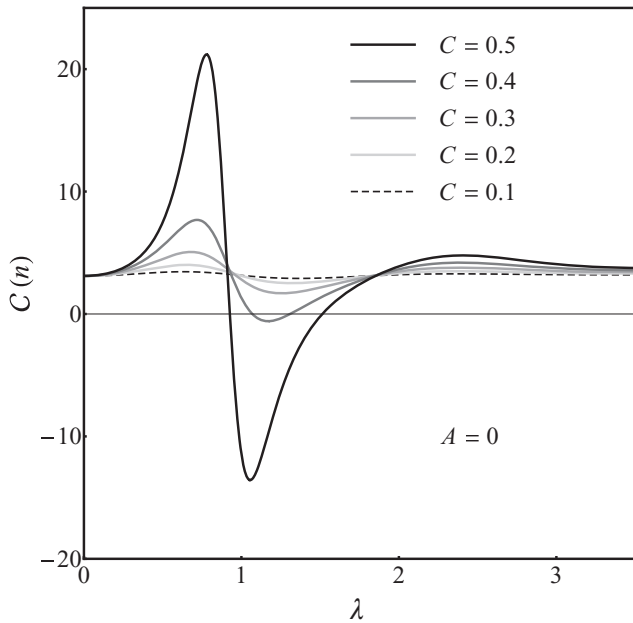


FIG. 6. Finger competition function $\mathcal{C}(n)$ plotted in terms of λ , for $B = 2.5 \times 10^{-3}$, $A = 0$, and five values of C .

terface [19]. Interestingly, the viscosity contrast influences the finger competition in an almost identical manner, regardless of the values of λ . Note that the slope of the lines for different λ in Fig. 7 shows minor variations. This further demonstrates that the finger competition is governed by a partial decoupling between elastic and viscosity parameters, characterized by a superposition of elastic dominant nonmonotonic effects with the linear monotonicity arising from viscosity contribution. Furthermore, the region delimited by the curves $\lambda = 0.8$ and $\lambda = 1.05$ provides a map in the parameter space (λ, A) for all

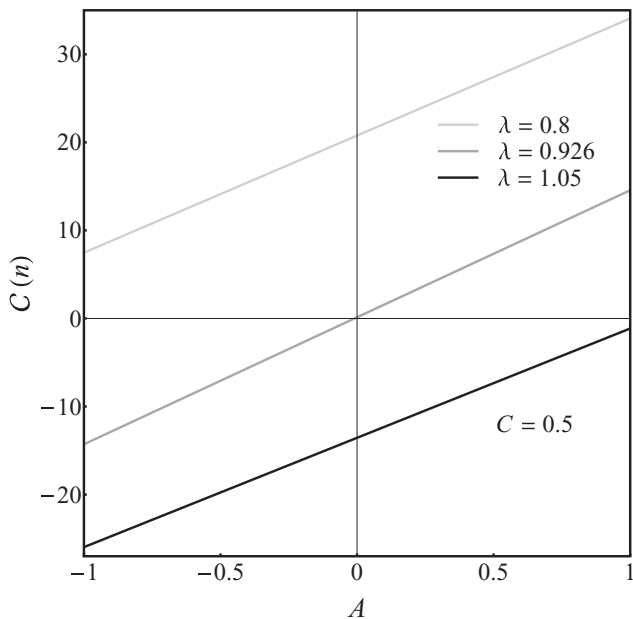


FIG. 7. Finger competition function $\mathcal{C}(n)$ as a function of the viscosity contrast A , for $C = 0.5$, and three different values of λ . These are the values of λ utilized to get the interfacial evolutions presented in Figs. 4 and 5.

possible finger competition morphologies, recalling that the values of λ that maximize or minimize $\mathcal{C}(n)$ do not depend on the viscosity contrast A , as shown in Fig. 3. Hence, the viscosity contrast A may be tuned to exacerbate, for instance, a desired competition behavior imposed by λ . Finally, C acts only to reduce the area between the curves $\lambda = 0.8$ and $\lambda = 1.05$ in Fig. 7, as deduced from Fig. 6.

After contemplating the findings of Figs. 5–7, we close this section by revisiting Fig. 4, and discussing it a bit further. One noteworthy feature of Fig. 4 is the rapid growth of the absolute value of the curvature for both inward- and outward-pointing fingers, together with the lack of symmetry between the curvature [as given by Eq. (6)] of inward- and outward-moving fingers for all values of λ . This is a direct consequence of the strong influence of the bending weakening effect while exponentially reducing the interfacial bending rigidity, which causes $\nu(\kappa)$ to reach its minimum value rapidly with $|\kappa|$, given the κ^2 dependence in Eq. (5). The variability in length between fingers is a result of a “tug of war” between outward- and inward-pointing fingers, Eqs. (15) and (16). The increased variability on the radial finger length depends on how rapidly a given finger (outward or inward) increases its mode amplitude, and consequently its local curvature, as expressed by Eqs. (15) and (16). In other words, outward- (inward-) growing fingers will compete if their curvature increases more rapidly than the inward- (outward-) moving finger.

Similarly, when the rate of growth of both inward and outward fingers are comparable, the finger competition is absent [see Eqs. (15) and (16)]. Nevertheless, the rate of bending rigidity decay is regulated by the characteristic curvature $1/\lambda$. This weakening effect on the bending rigidity tends to increase the curvature of a growing finger due to the locally reduced elastic bending resistance. When $\lambda = 0.8$ in Fig. 4(a), the outward fingers reach the minimum $\nu(\kappa)$ more rapidly than the inward fingers, since the initially circular shape of the interface forces inward fingers to switch the sign of the curvature before growing considerably, resulting in this way in a competition between outward-pointing fingers. When λ is increased to 0.926 in Fig. 4(b), a smaller magnitude of the absolute curvature now has access to lower bending rigidity values, favoring an equal rate of finger growth for both outward and inward fingers, and thus inducing zero finger competition phenomenon. Moreover, notice that the bending weakening effect does not privilege a particular sign of curvature, having therefore an equal effect for both outward- and inward-pointing fingers for the same magnitude of curvature. When the characteristic curvature is reduced further in Fig. 4(c), inward-moving fingers have faster access to the low bending rigidity values, resulting in an inward finger length variation, while considerably reducing the length of outward-moving fingers.

Finally, when λ is increased beyond 1.05, the bending weakening effect saturates at its minimum value very rapidly throughout the elastic interface, but for a small magnitude of curvature. In this case, the finger competition is solely governed by ν_0 , and the varying bending rigidity interface behaves as an interface with a constant bending rigidity [see Fig. 3]. In the latter, the viscosity contrast reemerges as the dominant parameter for the finger competition behavior, as expected from the classical rotating Hele-Shaw case [10–18].

IV. CONCLUDING REMARKS

Traditional studies of fingering instabilities in rotating Hele-Shaw cells have focused on the interplay of capillary, centrifugal, and viscous effects in dictating pattern formation behavior. In this framework, it has been shown that the viscosity contrast plays a major role in determining the finger competition dynamics of the system. If the viscosity contrast is positive (negative) the competition, or equivalently the finger length variability, among outward- (inward-) pointing fingers is increased. On the other hand, if the viscosity contrast tends to zero finger competition is restrained, so that both inward and outward pointing fingers have similar sizes.

Our current investigation, on the other hand, is concerned with a variant of the conventional rotating Hele-Shaw problem. Here we considered the situation in which the fluid-fluid interface is elastic and presents a curvature-dependent bending rigidity. In this new scenario, elastic, centrifugal, and viscous forces act to dictate the ultimate behavior of the emergent fingering structures. Through a second-order mode-coupling approach, we have derived the appropriate dimensionless form of the governing equations, containing four relevant parameters: a viscosity contrast A , a coefficient B that measures the relative strength between elastic and centrifugal effects, a rigidity fraction C , and a characteristic radius λ . In contrast to the usual rotating Hele-Shaw problem, our analytical results show a strong dependency of the finger competition dynamics on the parameters C and λ . The general observation is that, even if A and B are kept constant, by properly tuning the values of C and λ , one can reproduce a whole range of finger competition behaviors (i.e., enhanced competition among inward and outward fingers, or situations of restrained finger variability).

ACKNOWLEDGMENTS

J.A.M. and G.D.C. thank CNPq for financial support through the program “Instituto Nacional de Ciência e

Tecnologia de Fluidos Complexos (INCT-FCx),” and FACEPE through PRONEM project No. APQ-1415-1.05/10. H.G. acknowledges support from an Oxford University Hooke Fellowship and is supported by Award KUK-C1-013-04 from King Abdullah University of Science and Technology.

APPENDIX: FUNCTIONS APPEARING IN THE MODE-COUPLING TERM $F(n, m)$

This Appendix presents the expressions for the functions $B_1(n, m)$, $B_2(n, m)$, $B_3(n, m)$, and $B_4(n, m)$, which appear in Eq. (12):

$$B_1(n, m) = -3 + \frac{15}{4}m(n - m) + 10(n - m)^2 - \frac{9}{2}m^2(n - m)^2 - 6m(n - m)^3 - 4(n - m)^4, \quad (\text{A1})$$

$$B_2(n, m) = \frac{39}{2} - 30m(n - m) - 71(n - m)^2 + \frac{81}{2}m^2(n - m)^2 + 54m(n - m)^3 + 32(n - m)^4 - 12m^2(n - m)^4 - 12m^3(n - m)^3, \quad (\text{A2})$$

$$B_3(n, m) = -14 + 25m(n - m) + 54(n - m)^2 - 36m^2(n - m)^2 - 48m(n - m)^3 - 26(n - m)^4 + 18m^2(n - m)^4 + 18m^3(n - m)^3, \quad (\text{A3})$$

and

$$B_4(n, m) = 1 - 2m(n - m) - 4(n - m)^2 + 3m^2(n - m)^2 + 4m(n - m)^3 + 2(n - m)^4 - 2m^2(n - m)^4 - 2m^3(n - m)^3. \quad (\text{A4})$$

-
- [1] P. G. Saffman and G. I. Taylor, *Proc. R. Soc. London A* **245**, 312 (1958).
 - [2] G. M. Homsy, *Annu. Rev. Fluid Mech.* **19**, 271 (1987); K. V. McCloud and J. V. Maher, *Phys. Rep.* **260**, 139 (1995).
 - [3] L. Paterson, *J. Fluid Mech.* **113**, 513 (1981).
 - [4] H. Thomé, M. Rabaud, V. Hakim, and Y. Couder, *Phys. Fluids A* **1**, 224 (1989).
 - [5] J.-D. Chen, *J. Fluid Mech.* **201**, 223 (1989); *Exp. Fluids* **5**, 363 (1987).
 - [6] S. S. S. Cardoso and A. W. Woods, *J. Fluid Mech.* **289**, 351 (1995).
 - [7] O. Praud and H. L. Swinney, *Phys. Rev. E* **72**, 011406 (2005).
 - [8] J. A. Miranda and M. Widom, *Physica D* **120**, 315 (1998).
 - [9] S. W. Li, J. S. Lowengrub, and P. H. Leo, *J. Comput. Phys.* **225**, 554 (2007).
 - [10] L. W. Schwartz, *Phys. Fluids A* **1**, 167 (1989).
 - [11] Ll. Carrillo, F. X. Magdaleno, J. Casademunt, and J. Ortín, *Phys. Rev. E* **54**, 6260 (1996).
 - [12] E. Alvarez-Lacalle, J. Ortín, and J. Casademunt, *Phys. Fluids* **16**, 908 (2004).
 - [13] J. A. Miranda and E. Alvarez-Lacalle, *Phys. Rev. E* **72**, 026306 (2005).
 - [14] R. Folch, E. Alvarez-Lacalle, J. Ortín, and J. Casademunt, *Phys. Rev. E* **80**, 056305 (2009).
 - [15] C. Y. Chen, Y. S. Huang, and J. A. Miranda, *Phys. Rev. E* **84**, 046302 (2011).
 - [16] E. Alvarez-Lacalle, J. Ortín, and J. Casademunt, *Phys. Rev. E* **74**, 025302(R) (2006).
 - [17] J. Casademunt, *Chaos* **14**, 809 (2004).
 - [18] J. Casademunt, *Eur. Phys. J. Plus* **126**, 94 (2011), and references therein.

- [19] H. Gadêlha and J. A. Miranda, [Phys. Rev. E **70**, 066308 \(2004\)](#).
- [20] C.-Y. Chen, C.-H. Chen, and J. A. Miranda, [Phys. Rev. E **73**, 046306 \(2006\)](#).
- [21] T. Podgorski, M. C. Sostarecz, S. Zorman, and A. Belmonte, [Phys. Rev. E **76**, 016202 \(2007\)](#).
- [22] A. He, J. S. Lowengrub, and A. Belmonte, [SIAM J. Appl. Math. **72**, 842 \(2012\)](#).
- [23] A. He, Ph.D. thesis, Penn State University, 2011.
- [24] G. D. Carvalho, J. A. Miranda, and H. Gadêlha, [Phys. Rev. E **88**, 053006 \(2013\)](#).